sciendo

DOI 10.2478/ama-2019-0023

acta mechanica et automatica, vol.13 no.3 (2019)

SIMULATION AND ANALYSIS OF A TURBULENT FLOW AROUND A THREE-DIMENSIONAL OBSTACLE

Lamia BENAHMED*, Khaled ALIANE*

*Faculty of Technology, Department of Mechanical Engineering, University of Tlemcen, Bp 230, Chetouane Tlemcen, Algeria.

Benahmed_lamia91@yahoo.fr, kh_aliane@yahoo.fr

received 14 March 2019, revised 23 September, accepted 25 September

Abstract: The study of flow around obstacles is devised into three different positions: above the obstacle, upstream of the obstacle, and downstream of the latter. The behaviour of the fluid downstream of the obstacle is less known, and the physical and numerical modelling is being given the existence of recirculation zones with their complex behaviour. The purpose of the work presented below is to study the influence of the inclined form of the two upper peaks of a rectangular cube. A three-dimensional study was carried out using the ANSYS CFX calculation code. Turbulence models have been used to study the flow characteristics around the inclined obstacle. The time-averaged results of contours of velocity vectors <V>, cross-stream <v> and stream wise velocity <u> and streamlines were obtained by using K-ω shear -stress transport (SST), RANG K-ε and K-ε to model the turbulence, and the governing equations were solved using the finite volume method. The turbulence model K-ω SST has presented the best prediction of the flow characteristics for the obstacle among the investigated turbulence models in this work.

Key words: Turbulent flow, Obstacle, Finite volume, Turbulence models, ANSYS-CFX

1. INTRODUCTION

The generation of the turbulence within a channel was usually caused by the presence of baffles and obstacles. In the presence of obstacles, fluid flow, widely used in industry and application is extremely diverse. We can meet in the case of environmental problems related to the dispersion of pollutants through the cities and the effects of wind on buildings, ventilation road tunnel, the cooling fins of heat flares (Aliane et al., 2003), the baffles in heat exchangers or solar collectors, urban pipelines and so on. The study of the flow around obstacle may be the following two approaches. The digital approach is to discretise the governing equation of the flow by a digital method using different formulations (Hadjoui et al., 2003; Bitsuamiak et al., 2006). The experimental approach can be treated in two aspects; first is the qualitative where visualisation techniques are used to analyse the different nascent vortices within the flow (Sebbane et al., 2003). The second aspect is quantitative. For several years now, a large number of experimental and, more recently, numerical studies have concentrated on understanding complex flows around different profiled or not profiled obstacle models. This type of flow is generally found in many industrial applications, such as the cooling of electronic components (Saleha et al., 2015), atmospheric flows around buildings (Hainesa and Taylor, 2018), and fins of turbo machines. Several studies have been carried out on the application of flows around obstacles.

Hwang and Yang (2010) have carried out a numerical study on swirl (vortex) structures around a cube inside a canal. They found out that the number of vortices increased as the Reynolds number increased. Fillippini et al. (2005) investigated the case of the flow around cubes placed into a channel, using the large eddy simulation (LES) model. The results obtained showed that when the ratio S/H increases, the average drag coefficient augments for the second cube, while it remains approximately constant for the first one. Chang Lim et al. (2009) and Krajnovi'c and Davidson (2002) using the standard (LES) model provided a numerical simulation of the flow around a surface-mounted cube, placed in a turbulent boundary layer and comparing with experimentation. In the same approach, Yakhot et al. (2006) studied the turbulent flow around a bluff body. The immersed-boundary finite-volume method was introduced to carry out a direct numerical simulation. These same authors found out that the emergence of negative turbulence production in front of the cube can be used to explain the failure of some LES/RANS simulations in predicting the behaviour of flows around a surface-mounted cube. Becker et al. (2002) presented an experimental simulation using different aspect ratios in two different types of boundary layers to study the structure of the flow around three-dimensional obstacles. The experimental results showed that the flow structure around the obstacle depends on its aspect ratio, the angle of attack, Reynolds number and type of boundary layer. Aliane (2011) presented a numerical analysis of the turbulent flow of air inside a channel of rectangular section, with two types of obstacles: the first has a rectangular obstacle and another with a rounded upstream side having a radius of curvature equal to 0.2 times the height of the block. In the same approach, Rostane and Aliane (2015) conducted a three-dimensional study around two models of obstacles. The first one has a prismatic form, and the second one is prismatic and rounded downstream. The turbulence model k-ω shear-stress transport SST was used in this study. Hussein and Martinuzzi (1996) studied the effects of the flow field around a cube fixed on a wall. The authors focused on the velocity field, vortex, Reynolds stress, turbulent kinetic energy and turbulence dissipation in the backwash of the cube. Merahi et al. (2002) focused on the study of a three-dimensional and incompressible stationary

DOI 10.2478/ama-2019-0023

flow through a cascade of blades using a numerical simulation. The authors concluded that the losses because of the changes in the angle of incidence are the main cause of the decline in the performance of the turbomachines. Martinuzzi and Tropea (1993) used crystal violet, oil-film and laser-sheet visualisation techniques as well as static pressure measurements. The results have shown that the middle region of the wake is nominally two-dimensional for the width-to-height ratios greater than 6. Sarihassoun and Aliane (2016) studied the influence of the curved shape of the lover's edge of a rectangular obstacle. They compared two obstacle models using a qualitative approach, in which they analysed the dimensions of the recirculation zones, the velocity field and the kinetic energy and dissipation. Liao and Chen (2015) studied the velocity field of the flow beyond the obstacles using the particle image velocimetry technique using 8 μm Al_2O_3 powder as tracers. The flow field around the obstacles is obtained. The plots of the current lines and the average velocity field in the horizontal and vertical sections are drawn. The vortex characteristics of the wake flow in various flow fields are studied and compared. Basnet and Constantinescu (2017) conducted 3-D large-eddy simulations to study the physics of flow past 2-D solid and porous vertical plates of height H mounted on a horizontal surface with a fully developed, turbulent incoming flow. The simulation results are used to explain how the bleeding flow affects the dynamics of the larger billow eddies adverted in the separated shear layer (SSL) forming at the top of the plate and the wake structure. Sercan et al. (2017) investigated the flow characteristics around a surface-mounted cube at Re = 3,700 in terms of computational fluid dynamics (CFD) and then compared them with the experimental results using three different models of turbulence. Kanfoudi et al. (2017) used LES to present a numerical analysis of the turbulent flow structure induced by the cavitation shedding. Djeddi et al (2013), simulated a viscous fluid flow on an unconventional diamond-shaped obstacle in a confined channel that is simulated in low-to-moderate Reynolds numbers. The diamond-shaped obstacle is geometrically modified to represent different blocking coefficients depending on the height of the channel and different aspect ratios based on the length-to/height ratios of the obstacle. The simulations are divided into two stationary and unsteady flow groups. Liakos and Malamatris (2014) performed a direct numerical simulation (DNS) of steady-state laminar flow over a cube at Reynolds numbers ranging from 1 to 2,000 based on the cube height. In the same work, Diaz-Daniel et al. (2017) presented a DNS of a wall-attached cube immersed in laminar and turbulent boundary layers at various Reynolds numbers ReH ranging from 500 to 3000. In addition, Sumner et al. (2015, 2017) assessed the effect of the aspect ratio and the incidence angle of the flow above the free end of a surface-mounted finite cylinder and finite-height square prism, and Vinuesa et al. (2017) performed a DNS of the flow around a wall-mounted square cylinder under various inflow conditions and provide the effect of inflow conditions by considering a fully turbulent zero pressure gradient boundary layer. Shinde et al. (2015) presented a LES of flow over a wall-mounted cube-shaped obstacle placed in a spatially evolving boundary layer to understanding how variations in the cube height h modify the flow dynamics for the situation where the cube is within the boundary layer. Amraoui and Aliane (2018) presented the study of fluid flow and heat transfer in solar flat plate collectors by using CFD reduces time and cost. Ennouri et al. (2019) studied the modelling and simulation of the flow inside a centrifugal pump through non-cavitating and cavitating conditions using an SST-(SAS) turbulence model.

2. PROBLEMATIC

The present work contributes to the study of turbulent, stationary, three-dimensional, incompressible flow around a cube that has inclined upstream and downstream edges, mounted inside a horizontal channel. The ANSYS CFX-13 calculation code is used to simulate our configuration. The turbulence models (K-ω SST RANG K-ε and, K-ε) were used, and the governing equations were solved using the finite volume method.

3. MATHEMATICAL FORMULAS

The averaged equations of conservation of mass, momentum and energy are

- The mass conservation equation:

$$\frac{\partial \rho}{\partial t} + \frac{\partial (\rho U_i)}{\partial x_i} = 0 \tag{1}$$

- Momentum conservation:

$$\frac{\partial U_i}{\partial t} + U_j \frac{\partial U_i}{\partial x_j} = -\frac{1}{\rho}\frac{\partial P}{\partial x_i} + \upsilon \frac{\partial^2 U_i}{\partial x_j \partial x_j} \tag{2}$$

- Energy equations:

$$\frac{\partial \overline{T}}{\partial t} + \overline{U}_j \frac{\partial \overline{T}}{\partial x_j} = \frac{\partial}{\partial x_j}\left[\left(\frac{\mu}{\mathrm{Pr}} + \frac{\mu_t}{\mathrm{Pr}_t}\right)\frac{\partial \overline{T}}{\partial x_j}\right] + \frac{1}{\rho C_P}\Phi \tag{3}$$

- Reynolds equations:

$$\rho \frac{\partial \overline{U_i}}{\partial t} + \rho \overline{U}_j \frac{\partial \overline{U_i}}{\partial x_j} = -\frac{\partial \overline{P}}{\partial x_i} + \frac{\partial}{\partial x_j}\left(\mu \frac{\partial \overline{U_i}}{\partial x_j} - \rho \overline{u'_i u'_j}\right) \tag{4}$$

3.1. Model K-ω SST

The model SST is derived from the standard k-ω model. This model combines the robustness and accuracy of the formulation of the k-ω model in the near-wall region with the k-ε model and all its types for the free flow away from the wall. The definition of the turbulent viscosity is modified to take into account the transport of turbulent shear stresses. The formulation of the two-equation model is

$$\rho \frac{\partial k}{\partial t} + \rho \overline{U}_j \frac{\partial k}{\partial x_j} = \tilde{P}_k - \rho C_\mu \omega k + \frac{\partial}{\partial x_j}\left[(\mu + \mu_t/\sigma_k)\frac{\partial k}{\partial x_j}\right] \tag{5}$$

Specific dissipation rate:

$$\rho \frac{\partial \omega}{\partial t} + \rho \overline{U}_j \frac{\partial \omega}{\partial x_i} = 2\alpha\rho S_{ij} S_{ij} - \beta\rho\omega^2 + \frac{\partial}{\partial x_j}\left[\left(\mu_t + \sigma_\omega \mu_t\right)\frac{\partial \omega}{\partial x_j}\right] + 2(1 - F_1)\rho\sigma_{\omega 2}\frac{1}{\omega}\frac{\partial k}{\partial x_j}.\frac{\partial \omega}{\partial x_j} \tag{6}$$

The blend function F_1 is defined using the following equation:

$$F_1 = \tanh\left\{\left\{\min\left[\max\left(\frac{\sqrt{k}}{C_\mu \omega L}, \frac{500\upsilon}{L^2\omega}\right), \frac{4\rho\sigma_{\omega 2}k}{CD_{k\omega}L^2}\right]\right\}^4\right\} \tag{7}$$

Eddy viscosity is given by the following equation:

$$\upsilon_t = \frac{\alpha_1 k}{max(\alpha_1 \omega, \sqrt{2} S_{ij} F_2)} \quad (8)$$

The second blending function is defined using the following equation:

$$F_2 = \tanh\left[\left[\max\left(\frac{2\sqrt{k}}{C_\mu \omega L}, \frac{500\upsilon}{L\omega^2}\right)\right]^2\right] \quad (9)$$

To prevent the accumulation of turbulence stagnation regions, limited production was used:

$$\tilde{P}_k = \min\left(P_k, 10.\, C_\mu \rho k \omega\right) \quad (10)$$

$$P_k = \mu_t \frac{\partial U_i}{\partial x_j}\left(\frac{\partial U_i}{\partial x_j} + \frac{\partial U_j}{\partial x_i}\right) \quad (11)$$

The model constants are calculated using the mixing function

$$\text{F1:} \quad \phi = F_1 \phi_1 + (1 - F_1)\phi_2 \quad (12)$$

The values of the model constants are C_μ=0.09, α_1=5/9, α_2=0.44, β_2 =0.0828, σ_{k_1}=0.85, σ_{k_2}=1.0, σ_{ω_1}=0.5 and σ_{ω_2}=0.856.

3.2. Turbulence model k-ε

To close the system of equations of the problem to be solved and for a much more practical approach, we used the standard k-ε turbulence model (Jones and Launder, 1972); this model is a semi-empirical model with two transport equations based on the concept of Boussinesq linking the constraints of Reynolds to the average deformation rates:

- Turbulent kinetic energy *k*:

$$\frac{\partial}{\partial t}(\rho\kappa) + \frac{\partial}{\partial x_i}(\rho\kappa u_i) = \frac{\partial}{\partial x_i}\left[\frac{\left(\frac{\mu+\mu_t}{\sigma_\kappa}\right)\partial\kappa}{\partial x_i}\right] + P_\kappa + P_b - \rho\varepsilon - Y_M + S_\kappa \quad (13)$$

- Energy dissipation ε:

$$\frac{\partial}{\partial t}(\rho\varepsilon) + \frac{\partial}{\partial x_i}(\rho\varepsilon u_i) = \frac{\partial}{\partial x_i}\left[\left(\mu + \frac{\mu_t}{\sigma_\varepsilon}\right)\frac{\partial\varepsilon}{\partial x_i}\right] + C_{1\varepsilon}\frac{\varepsilon}{\kappa}(P_\kappa + C_{3\varepsilon}P_b) - C_{2\varepsilon}\rho\frac{\varepsilon^2}{k} + S_\kappa \quad (14)$$

P_k represents the term kinetic energy production:

$$P_\kappa = -\rho u_i u_j \frac{\partial u_j}{\partial x_i} \quad (15)$$

The turbulent viscosity is calculated by using the following equation:

$$\mu_t = \rho c_\mu \frac{\kappa^2}{\varepsilon} \quad (16)$$

The five empirical constants of the standard model of turbulence k-ε are

- σ_ε dissipation energy: ∂ε=1.3
- σ_k the Prandtl number of the turbulent kinetic energy: σ_k=1.0
- $C_\mu = 0.09 \quad C_{\varepsilon 1} = 1.44 \quad C_{\varepsilon 2} = 1.92$

4. MODEL DESCRIPTION AND COMPUTATIONAL DOMAIN

The obstacle used in our problem studied (Fig. 1) represents a cube that has inclined upstream and downstream edges, mounted inside a horizontal channel of length (L) and height (h) (Fig. 2)

4.1. Boundary conditions

As the flow is turbulent, three models of turbulence were chosen to analyse the problem more precisely. All "walls" are adiabatic and have no slip conditions.

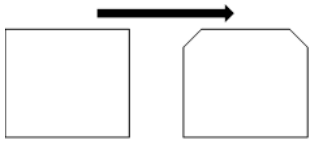

Fig. 1. Model of the body (plan view)

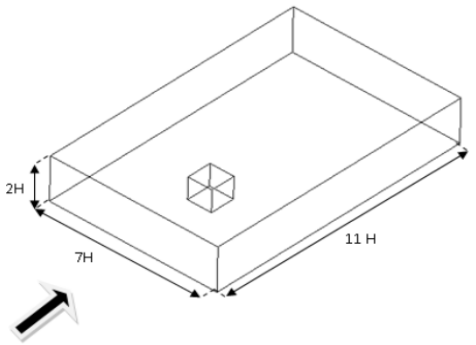

Fig. 2. 3D view of the computational domain of the cube (Rostane and Aliane, 2015)

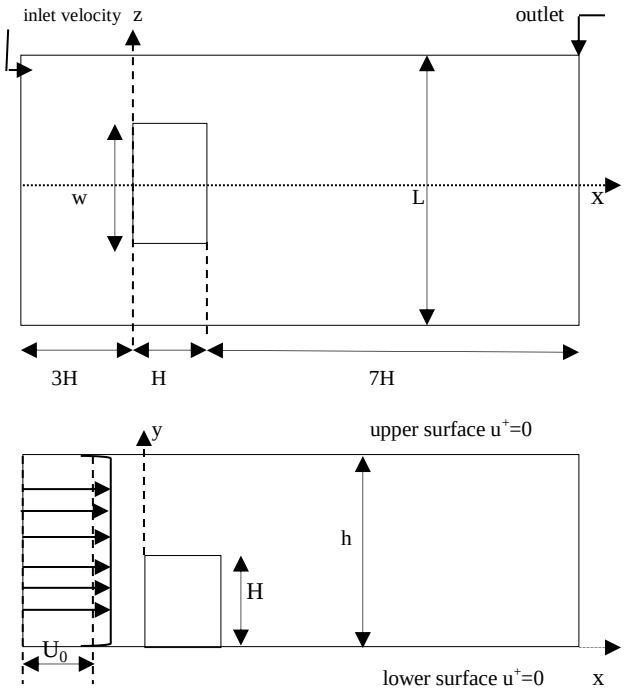

Fig. 3. Geometry of computational domain

DOI 10.2478/ama-2019-0023

According to the models selected previously, equations had to be solved using the following factors:

- The incoming flow velocity U_0 corresponds to the Reynolds number 8.10^4 ($Re=U_0.h/\nu$) and the channel height (h). The height of the obstacle is H=25 mm, and the channel height is h=2H.
- The velocity is zero u=0m/s near the lower and upper walls of the channel and above the obstacle. At the outflow, constant pressure imposed $P_{out}= 0$.

The boundary conditions of the problem treated are given in Figure 3.

To obtain a better precision of the results, it is necessary to generate a well refined mesh. It opted for a structured hexahedral mesh in our case. The meshing of the domain was performed using ANSYS CFX. The general practice is to use fine mesh size in areas of small changes in domain geometry. Figure 4 shows the grid of the mesh used.

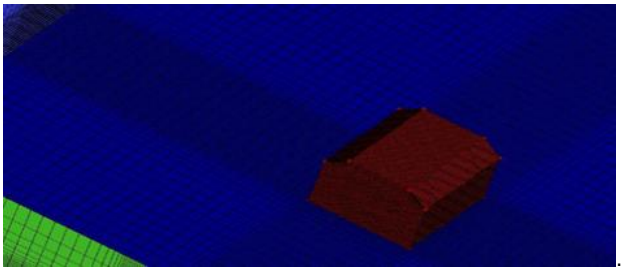

Fig. 4. The mesh grid configuration.

5. FLOW STRUCTURES

The flow above the wall-mounted cube presents a complex phenomenon such as the horseshoe tourbillon, the recirculation zones on the top and the back of the cube, illustrated in Figures 4 and 5. The presence of the obstacle causes the separation of the flow of fluid and the cube in these faces. The flow forms a recirculation zone near these faces, which increases the intensity of the turbulence. With the separation of the fluid flow in the mentioned areas, the fluid velocity increases progressively until it is attached to the near-back edge on the lateral and upper faces. The length of the recirculation zone on the upper face was indicated by L3 in Figure 5. The reinsertion of the flow on the cube takes place at the downstream corners of the upper face and the downstream corner on both sides of the face higher. A large region of separation develops behind the cube, which interacts with the horseshoe vortex. The length of this region was shown with L1. In Figure 6, three-dimensional, unstable and complex circulations in this region increase the intensity of the turbulence.

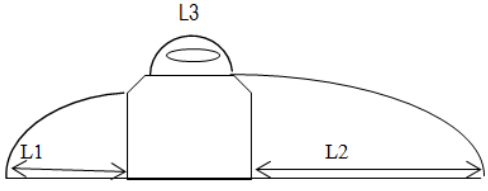

Fig. 5. Flow pattern around an inclined cube attached to the wall with three vortex lengths

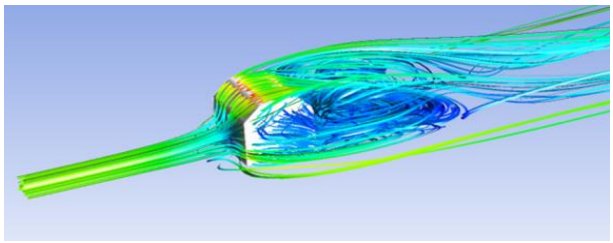

Fig. 6. Time-averaged streamlines around a wall-mounted inclined cube

6. RESULTS AND DISCUSSION

In this study, the flow domain carried out experimentally by Martinuzzi and Tropea (1993) has been prepared to validate the flow characteristics of the surface-mounted cube with a height of H=25mm placed in a channel height of h=2H. The structure of the flow around the obstacle has been validated by the work of Hussein and Martinuzzi (1995) for a Reynolds number of $Re=8{,}0\times10^4$ (Fig.7a). Upstream of the obstacle, a portion of the fluid remains blocked and we observed a small recirculation zone (point (a) to the result of Hussein and Martinuzzi (1995) and point (a') in our results Fig.7b), downstream of the obstacle appears as a large vortex as clearly seen by the two figures (point (b) to the result of Martunizzi and Hussein and point (b') in our results) and above the obstacle, the separation is triggered; it was caused by the upstream stopping point of the obstacle (point of reattachement) (point (c) to the result of Martinuzzi and Hussein and point (c') in our results). The comparison between the two simulations shows that the results are satisfactory and encouraging.

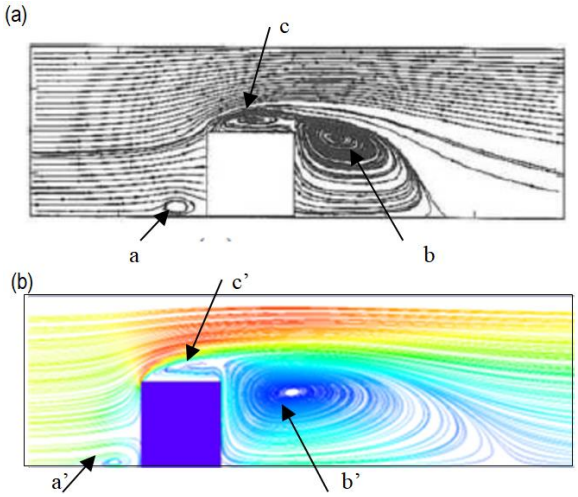

Fig. 7. Streamlines velocity on the symmetry plane at $Re= 8.10^4$ (a): Exp Hussein and Martinuzzi (1995), (b): k- ω SST

The study of the influence of the inclined form of the two upper peaks of a rectangular cube has been examined. A three-dimensional study was carried out using the ANSYS CFX calculation code. Three turbulence models have been used to study the flow characteristics around the inclined cube (K-ω SST, RANG K-ε and K-ε) at the Reynolds number of $Re=8.10^4$. The time-averaged and normalised results of velocity vectors fields <V>, transversal velocity <v> and longitudinal velocity <u> on the symmetry plane (z=0) around the obstacle have been presented in Figure 8.

The velocity vector fields <V> around the surface-mounted body have been illustrated in Figure 8 on the XY plane of the flow

DOI 10.2478/ama-2019-0023

domain and exactly on the plane of symmetry. From Figure 8, the flow has been triggered above the cube and more precisely on the inclined side. We clearly show that the flow was strongly accelerated in the zone above the obstacle. Visibly, the presence of a block inside the channel reduces the flow area causing a strong acceleration of the flow. However, the flow zone was formed for each turbulence model used in our study.

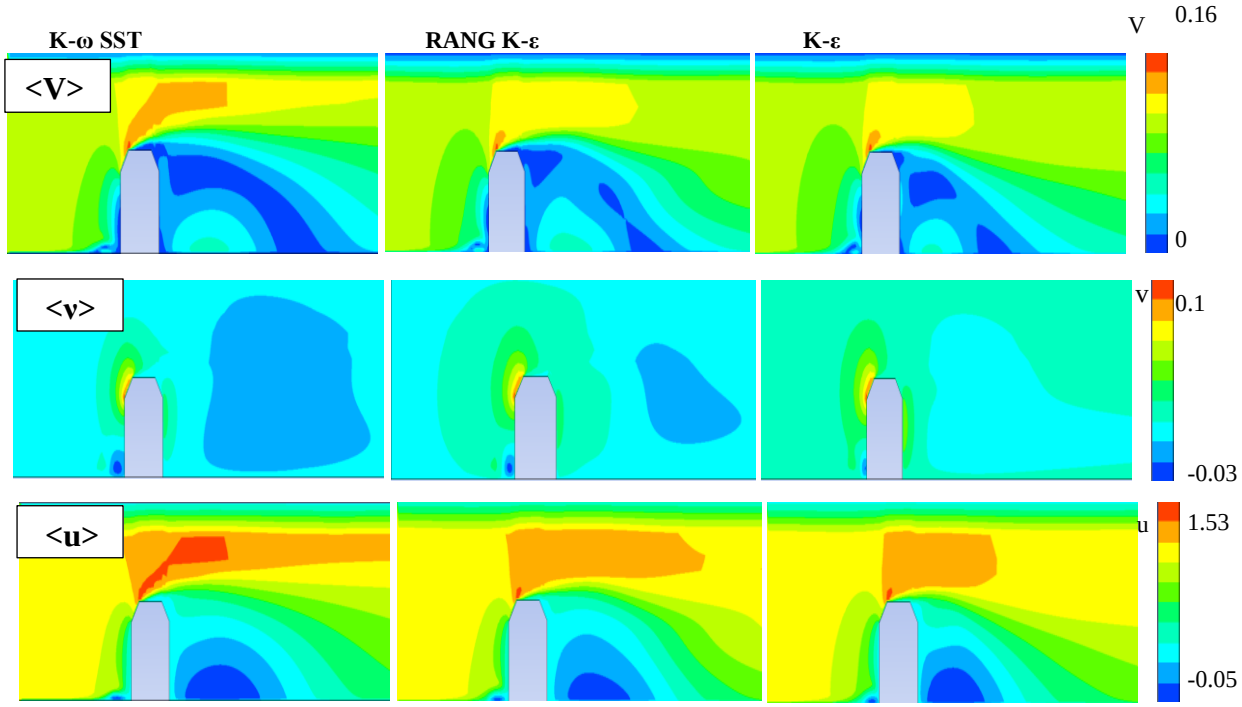

Fig. 8. Comparison of time-averaged results of contours of velocity vectors <V>, cross-stream velocity <v> and streamwise velocity <u> on the symmetry plane (z=0) at Reynolds number (Re=8.10^4)

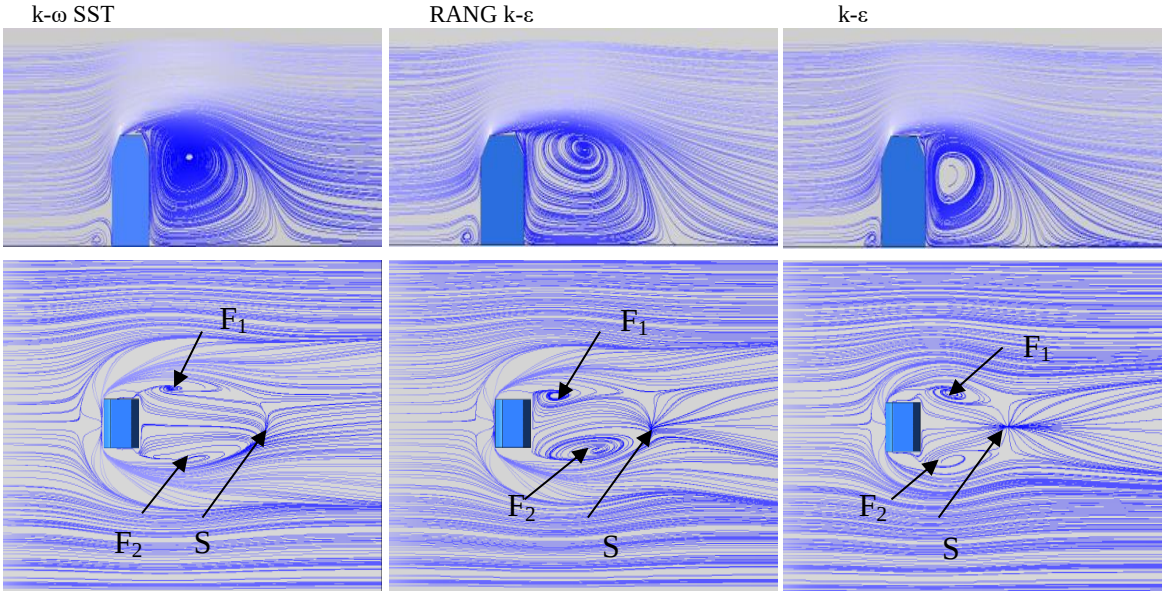

Fig. 9. Time-averaged streamlines on the symmetry plane and at the floor of the channel at the Reynolds number of Re=8.10^4

According to Figure 8, the largest flow area was obtained by the k-w SST method, while the turbulence model k-ε remained limited compared to the other methods.

The contours of the time-averaged streamwise velocity components <u> are presented in the range of -0.05 ≤ <u > ≤ 1.53 for the flow beyond the cube. We saw that the flow accelerated when arriving at the inclined part of the top of the cube and reaches a maximum value. The flux acceleration zone was superior in the case of the k-w SST method, whereas the turbulence model k-ε showed the narrowest. Also, the negative values of velocity components were observed after the cube with different cluster sizes.

The cross-stream velocity components <v > are presented in Figure 8 as 0.03 ≤ <v > ≤ 0.1 to Re = 8.10^4. The positive maximum values of the cross-stream velocity components are achieved above the obstacle and correctly on the inclination. The negative maximum values were dominant behind and upstream of the bottom of the cube.

DOI 10.2478/ama-2019-0023

For accurate flow analysis and for a good vision of separations and reattachments on the top of, at the lateral sides of and behind the obstacle, the time-averaged streamlines on the symmetry plane and at the floor of the channel at the Reynolds number of $Re=8.10^4$ for various turbulence models (K-ω SST, RANG K-ε and K-ε) were presented in Figure 9.

Streamlines on the symmetry plane was illustrated in Figure 8; upstream of the obstacle, a portion of the fluid remains blocked in the region between the inclined upstream edge and the bottom wall of the channel; we observe the formation of a large vortex downstream of the obstacle and above it and the separation is triggered; it is caused by the upstream stopping point of the obstacle, which is achieved for the three models of turbulence but the zone of recirculation was major in the case of the k-ω SST method, whilst the turbulence model k-ε showed the narrowest.

Figure 9 shows the streamlines at the floor of the channel; the blocking effect of the obstacle creates an unfavourable pressure gradient that separates the flow and moves away from the cube, forming a horseshoe vortex. For all models of turbulence, the horseshoe tourbillon appears upstream and bypasses the obstacle. On the other hand, there are two focus (F) points and one saddle (S) point achieved for all methods of turbulence.

In conclusion, it is stated that the turbulence model k-ε did not provide satisfactory results. Although the turbulence model RANG k-ε showed better results than the k-ε method, it remained behind the K-ω SST turbulence model with a narrow margin concerning the flow structure around the surface-mounted cube at $Re=8.10^4$.

6.1. Tracelines

In Figure 10, tracelines on the surface of the cube presented a steady flow in the high face and lateral sides. A separation of flux is observed in the middle of the front face forming a node. On the top of the cube and the high side, the flow is stable until the arrival of the inclined part of the cube; one sees a region of recirculation.

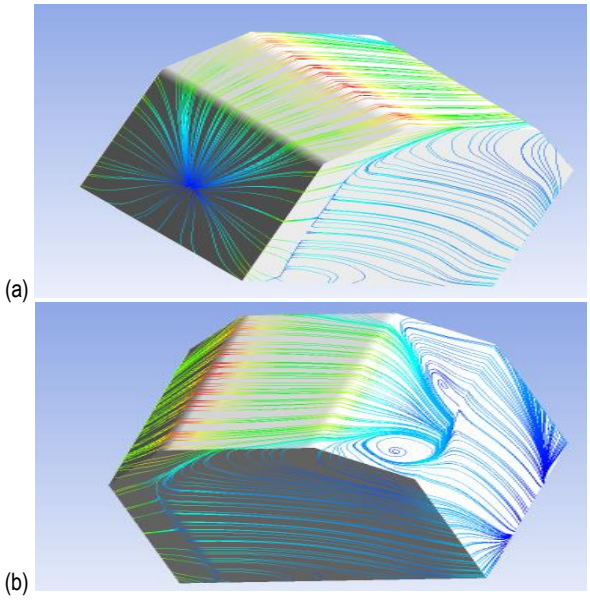

(a)

(b)

Fig. 10. Trace-lines on the surface of the cube: (a) front and side faces; (b) top and side faces

6.2. Streamribbons

Streamribbons are shown in Figure 11 and 12, where an exchange of fluid between the separation regions was observed. From these pictures, it can be concluded that the separation region around a three-dimensional bluff-body cannot be closed.

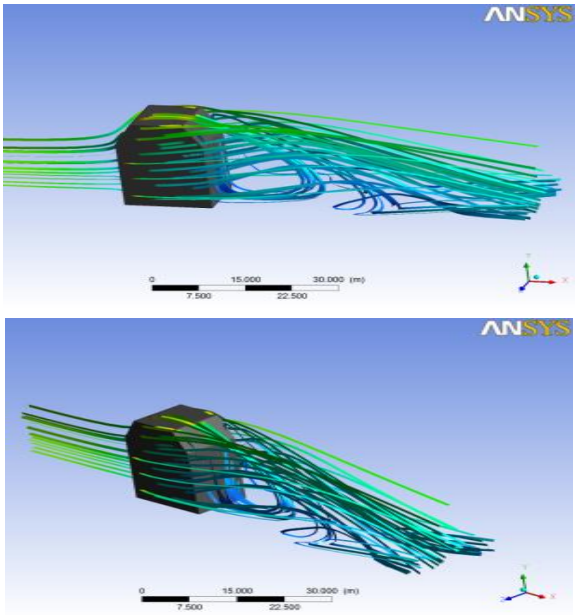

Fig. 11. Streamribbons: lateral and rear view

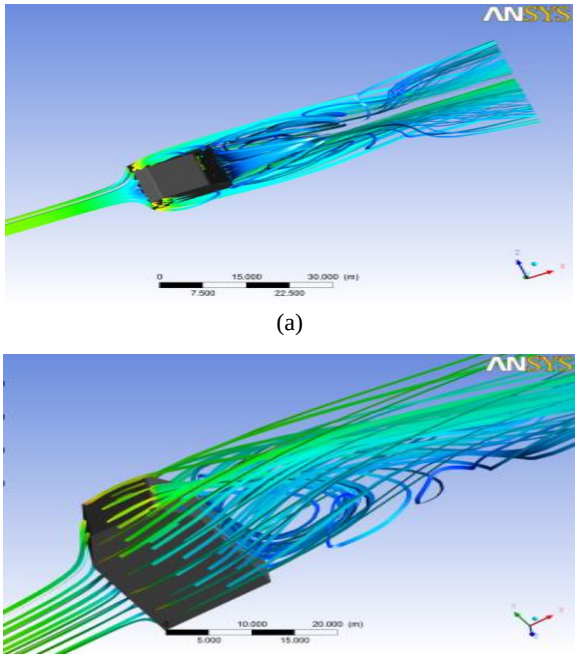

(a)

(b)

Fig. 12. Streamribbons: (a) lower view and (b) the lateral to the backward vortices

6.4. Iso-outline of mean Q-criterion

An overview of the mean flow is illustrated in Figure 13 and represents the isocontour of the mean dimensionless Q-criterion, Qi = 0.15. This criterion is a scalar invariant defined by the equation $Q=-\frac{1}{2} U_{i,j} U_{j,i}=-(\|S^2\| - \|\Omega^2\|)$ (Hunt et al. 1988). We can dimension the Q criterion using the equation $\bar{Q}= Q /(U_b/H)^2$.

Figure 13 shows the presence of a horseshoe vortex denoted by TFC, marginal vortices, denoted TM and wake vortices denoted TV. A sudden reflexion of the fluid is observed immediately after the obstacle. It is clear to see the nascent horseshoe vortex upstream of the obstacle and then the spacing of its legs when the inclined cube is exceeded.

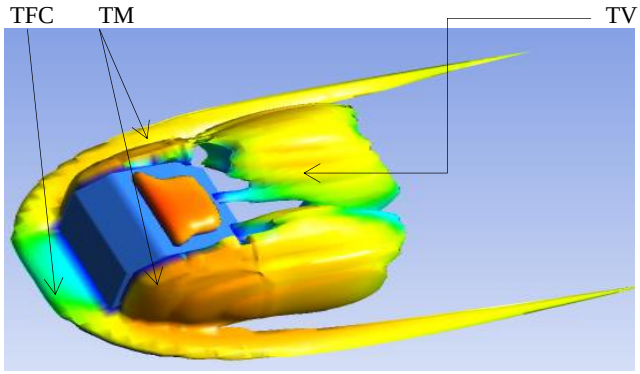

Fig. 13. Iso-outline of mean Q-criterion (Qi = 0.15).

7. CONCLUSION

The problem treated in this work is a three-dimensional simulation using the ANSYS CFX calculation code to carry out a three-dimensional numerical simulation of turbulent flow around an obstacle with inclined upstream and downstream edges. The flow characteristics of the surface-mounted cube as a function of the Reynolds number of Re = 8.10^4 has been studied with three different turbulence models. It has been explained that the satisfactory results have not been obtained using the k-ε and RNG k-ε methods and that the turbulence model k-ω SST gave better results after analyses as a function of time.

This study allowed a 3D simulation to analyse and understand some important physical aspects. In this type of flow, we especially tried to emphasise the role of the presence of obstacles in the channel, the distribution of dynamic and thermal exchanges. The analysis of simulation results confirms the following:

The presence of a block in the flow leads to an increase in the dynamic reciprocity and thus allows the improvement of heat transfer.

- An interaction between recirculation and main flow generates high turbulence; it has been marked in the strong velocity gradients and areas of high curvature trajectories upstream of the disturbance.

REFERENCES

1. **Aliane K**. (2011), Passive control of the turbulent flow over a surface mounted rectangular block obstacle and a rounded rectangular obstacle, International Review of Mechanical Engineering (IREME), 5(2), 305-314.
2. **Aliane K., Sebbane O., Hadjoui A.** (2003), Dynamic study of turbomachine blade cooling models, *Proceedings of the 11th International Day of Thermomics*, Algiers (Algeria), 315-320.
3. **Amraoui M.A., Aliane K. (2018),** Three-dimensional Analysis of Air Flow in a Flat Plate Solar Collector, *Periodica Polytechnica Mechanical Engineering*, 62(2), 126-135.
4. **Basnet K., Constantinescu G.** (2017), The structure of turbulent flow around vertical plates containing holes and attached to a channel bed, *Journal of Physics of Fluids*, 29, 115101.
5. **Becker H. Lienhart F.D.** (2002), Flow around three-dimensional obstacles in boundary layers, *J. Wind Eng. Ind. Aerodyn.*, 90, 265-279.
6. **Bitsuamlak G., Stathopoulos T., Bedard C.** (2006), Effects of upstream two-dimensional hills on design wind loads a computational approach, *Wind and Structures*, 9(1), 37–58.
7. **Diaz-Daniel C., Laizet S., Vassilicos J.** (2017), Direct Numerical Simulations of a wall-attached cube immersed in laminar and turbulent boundary layers, *International Journal of Heat and Fluid Flow (*Preprint submitted).
8. **Djeddi S.R., Masoudi A., Ghadimi P.** (2013), Numerical Simulation of Flow around Diamond-Shaped Obstacles at Low to Moderate Reynolds Numbers, *American Journal of Applied Mathematics and Statistics*, 1(1), 11-20.
9. **Dogan S., Yagmur S., Goktepeli I, Ozgoren M.** (2017), Assessment of Turbulence Models for Flow around a Surface-Mounted Cube, *International Journal of Mechanical Engineering and Robotics Research*, 6(3), 237-241.
10. **Ennouri M., Kanfoudi H., Bel Hadj Taher A., Zgolli R.** (2019), Numerical Flow Simulation and Cavitation Prediction in a Centrifugal Pump using an SST-SAS Turbulence Model, *Journal of Applied Fluid Mechanics*, 12(1), 25-39.
11. **Filippini G., Franck G., Nigro N.** (2005), Large Eddy Simulations of the flow around a square cylinder, *Mecanica Computacional*, XXIV A. Larreteguy (Editor), Buenos Aires, Argentina.
12. **Hadjoui A., Sebbane O., Aliane K., Azzi A.** (2003), Study of the appearance of swirling zones in a flow confronted with obstacles located at the entrance of a canal, *Proceedings of the 9th Congress of the French Society of Process Engineering*, Saint-Nazaire, (France), 224-229.
13. **Hainesa M., Taylor I.** (2018), Numerical investigation of the flow field around low rise buildings due to a downburst event using large eddy simulation, *Journal of Wind Engineering & Industrial Aerodynamics*, 172, 12-30.
14. **Hunt J.C.R., Wray A. A., Moin P.** (1988), *Eddies, stream and convergence zones in turbulent flows*, Technical report, Center of Turbulence Research.
15. **Hussein H.J., Martinuzzi R.J.** (1996), Energy balance for the turbulent flow around a surface mounted cube placed in a channel, *Phys. Fluids*, Vol. 8, No. 3, 764-780.
16. **Hwang J-Y, Yang K-S.** (2010), Numerical study of vertical structures around a wall-mounted cubic obstacle in channel flow, Physics of Fluids, 16(7), 2382-2394.
17. **Jones W.P., Launder B.E.** (1972), The prediction of laminarization with a two-equation model of turbulence, *International Journal of Heat and Mass Transfer*, 15, 301-14.
18. **Kanfoudi H., Bellakhall G., Ennouri M., Bel Hadj Taher A., Zgolli R.** (2017), Numerical Analysis of the Turbulent Flow Structure Induced by the Cavitation Shedding Using LES, *Journal of Applied Fluid Mechanics*, 10(3), 933–46.
19. **Krajnovi'c S., Davidson L.** (2002), Large-eddy simulation of the flow around a bluff body, *AIAA Journal*, 40(5), 927-936.
20. **Liakos A., Malamataris N.A**. (2014), Direct numerical simulation of steady state, three dimensional, laminar flow around a wall mounted cube, *Physics of Fluids*, 26(5), 053603.
21. **Liao B., Shan-Qun C.** (2015), Experimental study of flow past obstacles by PIV, *7th International Conference on Fluid Mechanics*, ICFM7, Procedia Engineering, 126, 537 – 541.

DOI 10.2478/ama-2019-0023

22. **Lim H.C., Thomas T.G., Castro I. P.** (2009), Flow around a cube in a turbulent boundary layer: LES and experiment, *Journal of Wind Engineering and Industrial Aerodynamics*, 97(2), 96–109.
23. **Martinuzzi R., Tropea C.** (1993), The flow around a surface-mounted prismatic obstacle placed in a fully developed channel flow, *J. Fluids Eng.*, 115, 85-92.
24. **Merahi.l , Abidat .M, Azzi.A, Hireche.O** (2002), Numerical assessment of incidence losses in an annular blade cascade, *Séminaire international de Génie Mécanique*, Sigma'02 ENSET, Oran.
25. **Nemdili S., Nemdili F., Azzi A.** (2015), Improving cooling effecti veness by use of chamfers on the top of electronic components, Microelectronics Reliability, 55(7), 1067-1076.
26. **Rostane B. , Aliane K.** (2015), Three Dimensional Simulation for Turbulent Flow Around Prismatic Obstacle with Rounded Downstream Edge Using the k-ω SST Model, *International Review of Mechanical Engineering* (I.RE.M.E.), 9(3), 266.277.
27. **Sari-Hassoun Z., Aliane K..** (2016), Numerical simulation of turbulent flow around obstacles with a curved upstream edge, International *Journal of Scientific Research & Engineering Technology* (IJSET), 196-201.
28. **Sebbane O., Hadjoui A., Aliane K., Azzi A.** (2003), New method of visualization of flows with very large Reynolds number, *Proceedings of the 9th Congress of the French Society of Process Engineering*, Saint -Nazaire, France, 259-264.
29. **Shinde S., Johnseny E., Makiz K.** (2017), Understanding the effect of cube size on the near wake characteristics in a turbulent boundary layer, *47th AIAA Fluid Dynamics Conference*, Denver, Colorado.
30. **Sumner D., Rostamy N., Bergstrom D., Bugg J**. (2015), Influence of aspect ratio on the flow above the free end of a surface-mounted finite cylinder, *International Journal of Heat and Fluid Flow*, 56, 290-304.
31. **Sumner D., Rostamy N., Bergstrom D., Bugg J.D.** (2017), Influence of aspect ratio on the mean flow field of a surface-mounted finite-height square prism, *International Journal of Heat and Fluid Flow*, 65, 1-20.
32. **Vinuesa R., Schlatter P., Malm J., Mavriplis C., Henningson, D.S.** (2015), Direct numerical simulation of the flow around a wall-mounted square cylinder under various inflow conditions, J*ournal of Turbulence*, 16, 555-587.
33. **Yakhot A., Liu H., Nikitin N.** (2006), Turbulent flow around a wall-mounted cube: A direct numerical simulation, *International Journal of Heat and Fluid Flow*, 27(6), 994-1009.